Modeling and Characterization of Deformable Soft Magnetic Microrobot for Targeted Therapy

Lyes Mellal, David Folio, Karim Belharet, Antoine Ferreira

Modeling and Characterization of Deformable Soft Magnetic Microrobot for Targeted Therapy

Lyès Mellal, David Folio, Karim Belharet and Antoine Ferreira

Abstract—Magnetic nanoparticles (MNPs) are very attractive components in many biomedical applications, particularly as therapeutic magnetic microcarriers (TMMC) for targeted therapy. Although MNPs can be effectively gathered and transported using external magnetic fields, the optimal delivery is yet to be fully investigated. In this paper, we discuss the modeling and the characterization of deformable soft magnetic microrobots under various magnetic field conditions. The microrobots considered consist of superparamagnetic iron oxide (SPIO) immersed in different carrier fluids, and the behavior of which has been characterized experimentally under weak magnetic fields. The experimental results clearly show that the observations properly follow the model prediction. Soft magnetic microrobots with controllable shape deformation have great potential for targeted drug delivery due to the adaptability of their characteristics to environmental conditions (e.g. vessel size, velocity, shear stress).

Index Terms—Deformable microrobot, magnetic actuation, magnetic microrobot, targeted therapy.

I. INTRODUCTION

Ferrofluids composed of magnetic nanoparticles (MNPs) have emerged as an important class of functional materials for many biomedical applications, with the potential to revolutionize current clinical diagnostic and therapeutic techniques. MNPs are already widely used as contrast agents in medical imaging [1], heating sources for hyperthermia treatments [2], tags for magnetic biosensing [3], and carriers for drug delivery [4]. A key advantage of MNPs is their capacity to be manipulated by an external magnetic field. MNPs have then been designed as components of therapeutic magnetic micro carriers (TMMC) for active and targeted therapy such as in confined environments [5], in fluid-filled cavities [6] and blood vascular system to treat vascular-related diseases ranging from vascular occlusion [7] to drug delivery [8, 9]. For instance, TMMC, also referred here as soft-microrobot, can effectively modify drug pharmacokinetics to decrease cytotoxicity in healthy tissues while increasing the releasing time and half-life of drugs [5, 7]. Obviously, one kind of bolus does not meet all clinical needs, and, thus, there is a need to select, design, and implement soft-microrobots that are matched to specific clinical indications and conditions [10]. To do so, a solution is to design biocompatible and controllable shape soft-microrobots by adapting its size with the vessels radii. In [11], the authors use thermoresponsive hydrogels with embedded MNPs for the implementation of shrinkable TMMC. This configuration allows them to shrink in response to temperature elevation caused by the embedded MNPs when exposed to an alternating magnetic field. A distinctive solution, inspired from transarterial chemoembolization (TACE), is to make the therapeutic agent to embolize the vessels of the targeted area (e.g. a tumor) where they then elute drugs in a locoregional manner, over a number of days to weeks [12]. To control the soft-microrobot, various external stimuli can trigger their on-demand assembly/disassembly, such as light [13], ultrasound [9], electric field [14] or magnetic field [15]. As example, the authors in [15] proposed an effective and reversible strategy for disassembling a vortex-like paramagnetic particle-based swarm using rotating magnetic fields.

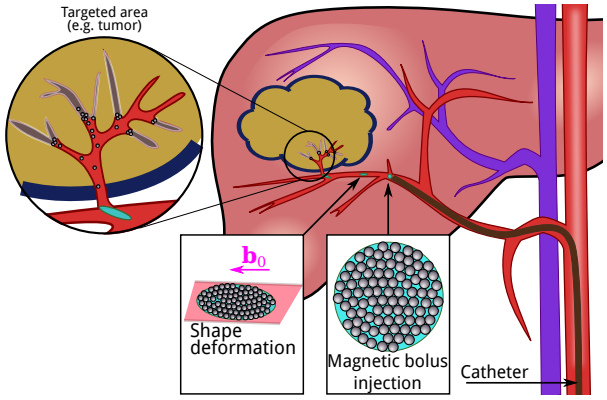

Fig. 1. Navigation of deformable soft magnetic microrobot delivered through a catheter for targeted therapy.

Strategy consisting to shape dynamically the soft-microrobots during the navigation to adapt their characteristics with respect to the applied magnetic field and the medium constraints is investigated here to improve targeted therapy. The considered concept is illustrated in Fig. 1. The idea is to use MNPs embedded in droplets to form a ferrofluid that is a deformable soft magnetic microrobot. Such soft-microrobots can then adapt their shape and response to their environment by exploiting their soft and stiff structures. To optimize the delivery of soft-microrobots, it is of great importance to understand their dynamics under different conditions and have a good knowledge of how each factor may affect their responses

David Folio and Antoine Ferreira are with INSA Centre Val de Loire, Univ. Orléans, PRISME EA 4229, France. lyes.mellal@insa-cvl.fr; david.folio@insa-cvl.fr; antoine.ferreira@insa-cvl.fr

Karim Belharet is with HEI - Campus Centre, PRISME EA 4229, France. karim.belharet@yncrea.fr

Digital Object Identifier (DOI): 10.1109/LRA.2021.3107102.

under varying magnetic fields [16]. Even though ferrofluid droplets have been studied for decades, to the authors' knowledge, very few studies address their explicit modeling as a soft-microrobotic system [17, 18, 19, 20]. Most of the existing works deal with either large droplets (e.g. $L > 1$ mm), or droplets moving on a substrate [18, 20]. Basically, the soft-microrobots differ in their properties (e.g. in size, shape, flexibility, coatings, magnetic loading, drug loading…), experience different forces even for the same applied magnetic field, and encounter different motion resistance for different body fluids, barriers, and tissue types. The contribution of this work lies in the study of the deformation of soft microrobots in viscous fluid subjected to an external magnetic field. Specifically, soft microrobots, made up of superparamagnetic iron oxide (SPIO) immersed in carrier fluid, are modeled and characterized experimentally. Let us notice that the present work aims to mainly address these two issues to identify the key aspects of their shape deformation and their response to the applied magnetic field.

The paper is organized as follows. Section II set out the model of deformable soft-magnetic boluses to highlight the relevant parameters. In Section III the methodology used in our works is presented, before showing the experimental characterization in Section IV. The paper is concluded with Section V.

II. MODELING

A. The Deformation of the Magnetic Bolus

In this study, a colloidal suspension of SPIO particles is used as deformable soft-magnetic microrobot. The soft-microrobot is then a ferrofluid droplet immersed in non-magnetizable medium. Each SPIO particle carry a magnetic moment. Without external magnetic field ($\mathbf{b} = 0$) their dipole directions are randomly spread, as illustrated in Fig. 2(a). In such situation, the ferrofluid droplet adopts commonly a spherical shape to minimize the surface energy. In presence of an applied magnetic field $\mathbf{b}$, the SPIO particles are polarized, and their magnetic moment are aligned with $\mathbf{b}$. During the magnetization process, the angle between the magnetic dipole moment and the magnetic field direction (i.e. $\theta - \varphi$ in Fig. 2(b)) becomes smaller as the magnetic field increases. Moreover, the field $\mathbf{b}$ induces a disturbance in the normal stress condition at the interface. Then, the soft-microrobot takes the shape of an ellipsoid, as shown in Fig. 2(b). Specifically, there is a competition between the magnetic energy of the SPIO particles which aim to be aligned with the field $\mathbf{b}$, and the surface energy which aims to keep the spherical shape. The deformation of the bolus depends mainly on the magnetic field $\mathbf{b}$ strength and the surface tension σ between the ferrofluid and the outer liquid. Commonly, the deformation is characterized with the dimensionless magnetic Bond number which is expressed as:

$$\mathcal{B}_{o\mathbf{m}} = \frac{\chi r_e}{2\mu_0 \sigma} |\mathbf{b}|^2 \tag{1}$$

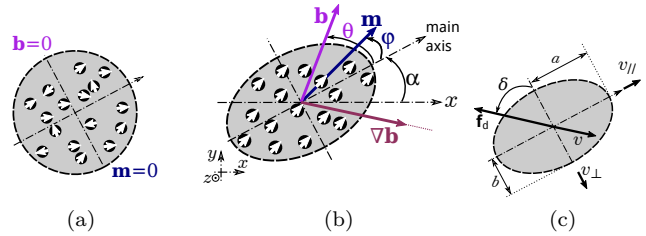

Fig. 2. Soft-magnetic microrobot: (a) without external magnetic field it exhibits a spherical shape; (b) with an external magnetic field $\mathbf{b}_0$ and gradient $\boldsymbol{\nabla}\mathbf{b}$ leads to an ellipsoidal shape. The black circles depict the SPIO particles with their magnetic moments $\mathbf{m}$ shown with the white arrows. (c) Representation of a prolate ellipsoid of revolution ($a < b = c$) with a the major semi-axis and b the minor semi-axis.

with $\mu_0 = 4\pi \times 10^{-7}\,\mathrm{T\,m\,A^{-1}}$ the vacuum permeability; r_e the radius of the soft-microrobot without magnetic field ($\mathbf{b} = 0$) or the equivalent spherical volume radius; χ the magnetic susceptibility of the material (considered here isotropic). $\mathcal{B}_{o\mathbf{m}}$ represents the ratio between magnetic and surface tension forces.

B. Magnetic Actuation of Soft-Magnetic Microrobot

The magnetic actuation of a body is obtained through the manipulation of a magnetic field $\mathbf{b} = (b_x, b_y, b_z)^\top$ to induce on its magnetized material volume $V_\mathrm{m} = \tau_m V$ (with τ_m the magnetization rate) a magnetic force $\mathbf{f_m}$ and torque $\mathbf{t_m}$, that is:

$$\mathbf{f_m} = V_\mathrm{m}\ (\mathbf{m}\cdot\nabla)\,\mathbf{b} \tag{2}$$

$$\mathbf{t_m} = V_\mathrm{m}\ (\mathbf{m}\times\mathbf{b}) \tag{3}$$

with $\mathbf{m} = (m_x, m_y, m_z)^\top$ the magnetization; ∇ the gradient operator and $\times$ the cross product.

Commonly, for hard magnetic materials the magnetization $\mathbf{m}$ is independent of the magnetic field $\mathbf{b}$, and could be considered easily saturated in many cases. In contrast, for soft-magnetic materials, as with using SPIO, $\mathbf{m}$ is strongly related to $\mathbf{b}$. At low magnetic fields, such that $|\mathbf{m}| < m_\mathrm{sat}$ (with m_sat the saturation magnetization of the material), the of SPIO particles exhibits typically the following magnetization [21]:

$$\mathbf{m} = \frac{\chi_a}{\mu_0(1+\chi)}\mathbf{b} \tag{4}$$

where $\chi_a \in \mathbb{R}^{3\times3}$ is the apparent susceptibility tensor that is related to the soft-microrobot shape. Here, the soft-microrobot varies from spherical geometry to axisymmetric prolate ellipsoid (see Fig. 2). For such spheroidal shape, the susceptibility tensor is expressed as follows:

$$\chi_a = \mathrm{diag}\left(\frac{\chi}{1+n_a\chi}, \frac{\chi}{1+n_b\chi}, \frac{\chi}{1+n_b\chi}\right) \tag{5}$$

where $n_a < 1$ and $n_b < 1$ are demagnetizing factors along the major and minor axis, such as: $n_a + 2n_b = 1$. For a prolate spheroid ($a > b = c$) we get [21, 22]:

$$n_a = \frac{1-\varepsilon^2}{2\varepsilon^3}\left(\log\left(\frac{1+\varepsilon}{1-\varepsilon}\right) - 2\varepsilon\right) \tag{6}$$

with $\varepsilon = \sqrt{1-\Lambda^{-2}} \in]0;1[$ the eccentricity, and $\Lambda = a/b$ the aspect ratio of the spheroidal soft-magnetic microrobot. In the case of spherical device the demagnetizing factors simplify to $n_a = n_b = \frac{1}{3}$.

Furthermore, the dimensionless magnetic Bond number (1) for ellipsoidal droplet ferrofluid is related to the aspect ratio as [18]:

$$\mathcal{B}_{\mathrm{o}\mathbf{m}} = \left(\frac{1}{\chi} + n_a\right)^2 \Lambda^{1/3}\left(2\Lambda - \Lambda^{-2} - 1\right) \tag{7}$$

This relation implies that, in the general case, the constitutive law (4) might be non-linear, as χ_a is varying with the aspect ratio Λ which is also function of $\mathbf{b}$ through the Bond number (1).

From Eqs. (2), (4), and (5), it is then straightforward to compute the magnetic force $\mathbf{f_m} = (f_{mx}, f_{my}, f_{mz})^\top$, which is here fully expressed as:

$$\begin{pmatrix} f_{mx} \\ f_{my} \\ f_{mz} \end{pmatrix} = \frac{V_{\mathrm{m}}\chi}{\mu_0(1+\chi)} \boldsymbol{\nabla}\mathbf{b} \begin{pmatrix} \frac{b_x}{1+n_a\chi} \\ \frac{b_y}{1+n_b\chi} \\ \frac{b_z}{1+n_b\chi} \end{pmatrix} \tag{8}$$

The optimization of this motive force depends on the knowledge and the control of three fundamental parameters: i) the volume of magnetic material V_{m}; ii) the magnetic field $\mathbf{b}$ and its gradient $\boldsymbol{\nabla}\mathbf{b}$; and iii) the demagnetizing factor (6) that is related to the aspect ratio Λ.

Secondly, Eq. (3) shows that the magnetic torque $\mathbf{t_m}$ tends to align the magnetization $\mathbf{m}$ with the applied field $\mathbf{b}$. As previously, from (3), (4) and (5), the magnetic torque is computed for a prolate ellipsoid of revolution in a low magnetic field, and we get:

$$\mathbf{t_m} = \frac{V_{\mathrm{m}}\chi^2}{2\mu_0} \frac{|1-3n_a|}{(1+n_a\chi)(1+n_b\chi)} \begin{pmatrix} 0 \\ b_x b_z \\ b_x b_y \end{pmatrix} \tag{9}$$

C. Hydrodynamic Force and Torque of Spheroidal Bolus

Assuming that the flow is incompressible, the drag force $\mathbf{f}_{\mathrm{d}}$ and torque $\mathbf{t}_{\mathrm{d}}$ on a spheroidal microrobot immersed in a Newtonian fluid is expressed in the general case as [23]:

$$\begin{pmatrix} \mathbf{f}_{\mathrm{d}} \\ \mathbf{t}_{\mathrm{d}} \end{pmatrix} = - \begin{pmatrix} \mathbf{K} & 0 \\ 0 & \boldsymbol{\Omega} \end{pmatrix} \begin{pmatrix} \mathbf{v} \\ \omega \end{pmatrix}, \tag{10}$$

with $\mathbf{v} = (v_x, v_y, v_z)^\top$ and $\omega = (\omega_x, \omega_y, \omega_z)^\top$ are respectively the linear and angular velocity of the soft-microrobot with respect to the fluid flow. The resistance matrix defined by $\mathbf{K}$ and $\boldsymbol{\Omega}$, is a symmetric matrix function of the properties of the flow and of the geometry of the microrobot. Moreover, the drag experienced by a spheroidal microrobot acts in the direction of motions $\{\mathbf{v}, \omega\}$, and is defined in creeping flow as [10]:

$$\mathbf{f}_{\mathrm{d}} = -6\pi\eta r_e \kappa_f \cdot \mathbf{v} \tag{11}$$

$$\mathbf{t}_{\mathrm{d}} = -8\pi\eta r_e^3 \kappa_{\mathrm{rot}} \cdot \omega \tag{12}$$

where η is the fluid viscosity; κ_f and κ_{rot} are dimensionless dynamic shape factor. In previous study, we have well-investigated these factors for spheroids, ellipsoid and chain-like of sphere TMMCs [10]. Especially, the dimensionless shape corrections depends on the direction of the movement: namely parallel $v_{//}$ or orthogonal $v_\perp$. In the following ellipsoidal shape with aspect ratio in the range $\Lambda \in [1;4]$ is considered. Such geometry leads to dynamic shape factor in the range of $[1; 1.59]$ in parallel motion, and $[1; 2.05]$ in orthogonal motion. Obviously, parallel motion of ellipsoidal shape is more efficient rather than following a perpendicular motion [10]. Hereafter, the parallel motion is mainly considered.

III. MATERIALS AND METHODS

A. Magnetic Bolus Preparation

The soft-microrobot is an heterogeneous mixture consisting of a colloidal liquid where SPIO particles (Fe_3O_4) are suspended in a carrier fluid, that will be in the end replaced with the therapeutic agent. Two phases can be differentiated: the carrier phase and the surrounding liquid. To mimic different types of drug load, here, SPIO are suspended either in aqueous or in oleaginous phase. The former consists of SPIO particles suspended in distilled water with particle concentration of 50 mg/ml (BioMag BM547, Bang Laboratories Inc.), and is referred as bolus-#A. Secondly, oil-based ferrofluid is designed with SPIO powder (Inoxia Ltd, UK) mixed with oil, referred as bolus-#B. Examples of these soft-microrobots are shown in the accompanying video. Sunflower oil, which is biocompatible, biodegradable, environmentally friendly, was selected as the oleaginous carrier liquid in the present work. The bolus-#B is an homemade ferrofluid that is prepared by mixing sunflower seed oil and the SPIO powder for 30 min in a volumetric ratio of $\tau_m = 60\%$ magnetic particles. This chosen τ_m ratio is related to the optimal magnetization rate that allows conveying an optimum drug load for bolus size in the order of radius of $r = 500\,\mu\mathrm{m}$ [10]. Then the density of the magnetic boluses is basically computed from:

$$\rho_{\mathrm{b}} = (\tau_m \rho_{\mathrm{p}} + \rho_{f/b}(1-\tau_m)) \tag{13}$$

with ρ_p the density of the SPIO particles, and $\rho_{f/b}$ the ferrofluid carrier fluid density. The bolus-#B is then immersed in mixture of distilled water and glycerol to investigate the impact of the variation of the medium viscosity. The relevant physical characteristics of considered liquids are summarized in Table I, and the properties of the two types of boluses are given in Table II.

B. Experimental Setup

The ferrofluid droplet is dispensed via a catheter (here a flexible needle) connected to a controlled syringe pump (Model KDS 200; KD Scientific, USA), and is depicted in Fig. 3. The control of the pump is provided by a computer using LabView (National Instruments, USA) software. The use of syringe pump ensures that the required soft-microrobot volume V is injected. It is possible to reliably control the number of soft-microrobot administered. Once, the soft-microrobot is injected, a high-resolution CCD

TABLE I
Physical properties of the different liquids media (at† $T = 20\,°C$)

Liquid mixture	Viscosity (mPa.s)	Density ρ_f (kg/m^3)
(#1) distilled water (W)	0.998	998
(#2) W+20% glycerin	1.740	1056
(#3) W+50% glycerin	6.000	1144
(#4) W+70% glycerin	23.090	1202
(#5) W+80% glycerin	60.860	1231
(#6) sunflower oil	62.000	920

† The experiments are conducted in air conditioned room.

TABLE II
Magnetic boluses properties (at† $T = 20\,°C$)

Bolus	Particle size r_p (μm)	Carrier fluid	Density ρ_b (kg/m^3)
#A (BioMag BM547)	5.0	#1 water	1208
#B (homemade)	0.2	#6 oil	3128

microscope camera (TIMM 400, Nanosensor) records the top view of the workspace. A robust tracking algorithm process the images flow to measure the location, the orientation and the shape of the soft-microrobot with a sub-micrometer resolution.

Finally, an electromagnetic actuation (EMA) system (Aeon Scientific, Switzerland) is used to control the magnetic microrobot. The EMA system consists of three nested sets of Maxwell coils and one nested set of Helmholtz coils. The EMA setup enables the induction of a magnetic field within the workspace of $20\,\text{mm} \times 15\,\text{mm} \times 10\,\text{mm}$. The generated magnetic fields and gradients vary linearly with the electrical currents flowing through the coils' wire that are controlled by a computer through a data acquisition board (NI PCI-6229) and LabVIEW® software. Commonly, Helmholtz coils are used to generate a uniform magnetic field, whereas its gradient remains negligible. Maxwell coils pair are commonly used to induce a uniform magnetic gradient field with current circulating in opposite direction. If the current flow in the same direction, a roughly uniform field $\mathbf{b}$ appears in the workspace.

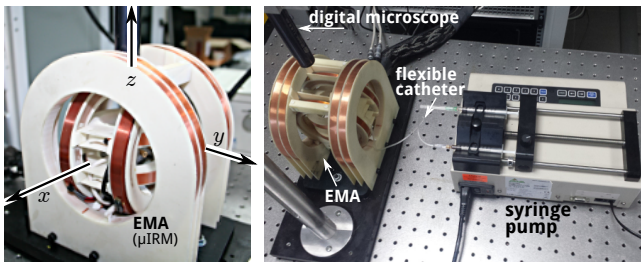

Fig. 3. The experimental platform that comprises: (left) the EMA coil set called μIRM, and (right) the soft-microrobots injector.

IV. EXPERIMENTAL CHARACTERIZATION

Different experiments have been realized to characterize the properties and behaviors of deformable soft-magnetic microrobots, and are reported hereafter.

A. Soft-microrobot Properties Without Magnetic Field

The two types of considered ferrofluids are injected in different liquids media. Here, the objective is to characterize the shape and properties of each soft-microrobots without any magnetic field ($\mathbf{b} = 0$). The water-based bolus-#A is stabilized in an oleaginous phase (sunflower oil) to get an immiscible behavior. Without magnetic field, the bolus shape remains spherical, with the aspect ratio $\Lambda = a/b = 1.009 \pm 1.3 \cdot 10^{-3}$ and the eccentricity $\varepsilon = 0.13$. The oil-based bolus-#B is placed in different aqueous solutions of glycerin. Once again, the soft-microrobot remains quasi-spherical. The Fig. 4(a) shows the evolution of aspect ratio Λ with respect to the viscosity $\eta_{f/m}$ of the various mixtures of water and glycerin to investigate different viscous media. For each fluid viscosity, the statistical data are processed from the recorded video of the soft-microrobot. These results exhibit that a high value of the viscosity $\eta_{f/m}$ implies an aspect ratio closer to $\Lambda = 1$, that is a better sphericity. Moreover, within low viscosity and without any specific coating, the magnetic bolus-#B tends to slightly crumble. These behaviors are related to the interfacial tension σ that is increasing with viscosity $\eta_{f/m}$, as reported in Fig. 4(b). The knowledge of the interfacial tension σ, between the soft-microrobots and the surrounding medium, is crucial for the understanding of the shape behavior evolution. To characterize σ, we consider the Taylor formula defined as [24]:

$$\sigma = \frac{g\lambda^2}{4\pi^2}\left(\rho_\text{b} - \rho_{f/m}\right) \tag{14}$$

where $g = 9.8\,\text{m}\,\text{s}^{-2}$ is the gravity acceleration; $\rho_{f/m}$ is the surrounding environment density (cf. Table I); and λ is the Taylor wavelength also referred as capillary length. The surface tension σ are determined by measuring the peak spacing (i.e. the Taylor wavelength) which appears when a sufficient magnetic field is applied. The obtained characterization of σ in Fig. 4(b) are consistent with interfacial tension of ferrofluid reported in other studies [17, 18].

B. Magnetic Bolus within a Uniform Magnetic Field

1) Magnetic Properties: The magnetization $\mathbf{m}$ of the two soft-microrobots has been experimentally evaluated. From the observed shape and motion, and the magnetic model of soft-magnetic microrobots presented in Section II-B, the magnetization is determined, and is reported as (circles) and (squares) in the Fig. 5. In our study, the microrobot is subject to a low static magnetic field, and the SPIO particles does not reach the magnetization saturation $m_\text{sat} \approx 15\,\text{kA/m}$. Therefore, the magnetization curves remains linear. Especially, without applied magnetic field ($\mathbf{b} = 0$) neither magnetic coercivity nor hysteresis is observed, underscoring the superparamagnetic

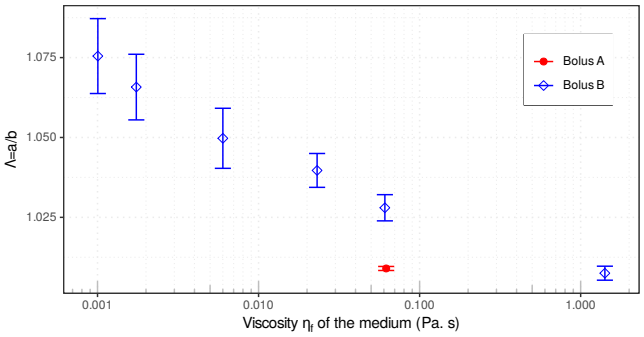

(a)

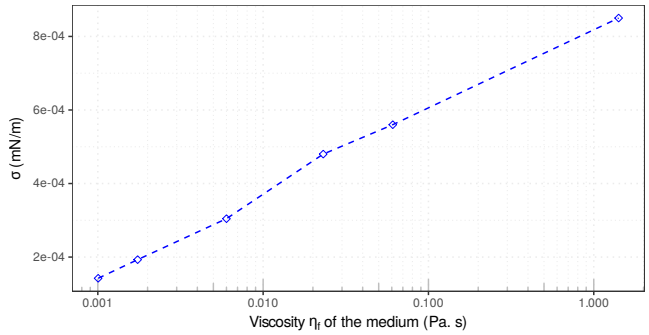

(b)

Fig. 4. Properties of the magnetic bolus in different fluid viscosity η_f: (a) the aspect ratio $\Lambda = a/b$, and (b) the interfacial tension σ.

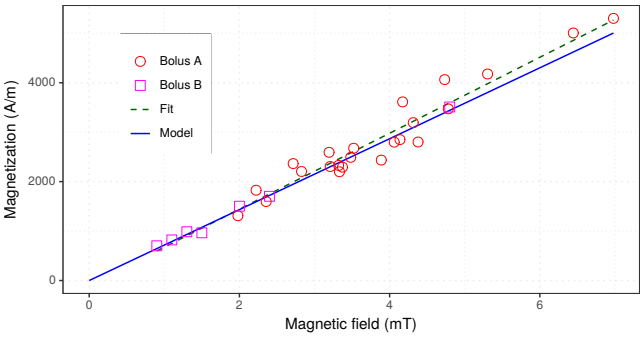

Fig. 5. Magnetization curves: (solid line) modeled from constructor data; (dashed) fitted linear regression from experiments using bolus-#A (circles) and #B (squares).

behavior of the SPIO particles. Secondly, the characterized values are close to the model (solid-line) computed from the constructor data (BioMag BM547, Bang Laboratories Inc.). In particular, the linear regression approximation (dashed-line) fits reliably the model's curve with a relative error less than $< 5.31\%$. Hence, the considered soft-magnetic model seems to accurately describe the behavior of the magnetic bolus.

Furthermore, the magnetization is related to the bolus magnetic susceptibility χ thanks to Eq. (4). The resulting data are shown in Fig. 6. On each box the central line represents the median values, the height of the box indicates the interquartile range between 25% and 75% percentiles of the measures, and the whiskers extend to the most extreme data points. As one can see, the bolus-#A denotes a more important variance than the

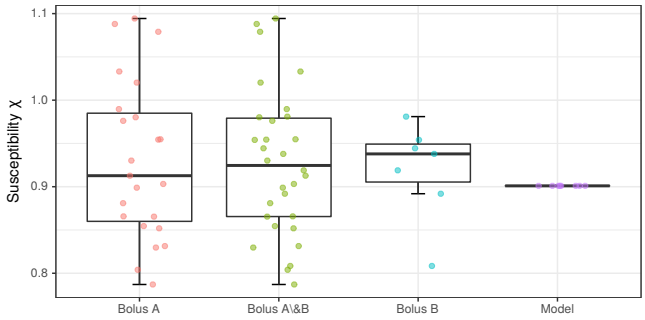

Fig. 6. Magnetic susceptibility retrieved from the model and from the measurement of bolus #A and #B.

bolus-#B. This is mainly related to the low level of magnetic material included in bolus-#A, that induces a low magnetic response and a scattering in the measured values. Secondly, at low magnetic fields, due to the strong surface tension, it is difficult to change significantly the shape of bolus-#A. Therefore, in the following the bolus-#B is mainly considered. Moreover, this evaluation of the magnetic susceptibility around $\chi = 0.91$ is consistent with value of 0.8903 reported in [18] for their ferrofluid droplet.

It can be noticed that, in our study, the volume variation of the magnetic bolus does not significantly modify the susceptibility. More precisely, this means that the ferrofluid carrier fluid (aqueous mixtures or oleaginous solution) have not a significant magnetic response and can be considered to be magnetically transparent.

2) Shape and Surface Properties: To experimentally evaluate the proposed modeling and methods, the home-made magnetic bolus-#B is hereafter solely considered. Hence, the oil-based bolus-#B is first injected in a square box filled with different viscous liquids (i.e. various aqueous solutions of glycerin, see Table I) which is placed within the workspace of the EMA system. Then, the influence of the applied magnetic field $\mathbf{b}$ on the ferrofluid droplet is investigated. Fig. 7 shows some snapshots of the bolus-#B immersed in an aqueous solution of 50% of glycerin with $\rho_f = 3\,\text{mPas}$, which corresponds to a fluid viscosity similar to the blood. As expected, an ellipsoid shape appears as the magnetic field is increasing. This behavior is related to the competition between the magnetic response of the SPIO particles which tend to be aligned with the magnetic field $\mathbf{b}$, and the surface energy which try to maintain a spherical shape.

Fig. 8 shows the evolution of the aspect ratio Λ of magnetic boluses as function of the magnetic field $\mathbf{b}$. As previously, the viscosity $\eta_{f/m}$ of the surrounding medium significantly influence the variation of the aspect ratio. As mentioned, the deformation evolution is due to the competition between the magnetic energy and the surface energy of the bolus.

The interfacial tension (14) of the magnetic boluses has been also evaluated experimentally for different liquid viscosity, and is shown in Fig. 9. As expected, the interfacial tension σ is increasing with the viscosity together with the applied magnetic field. As comparison the estimated

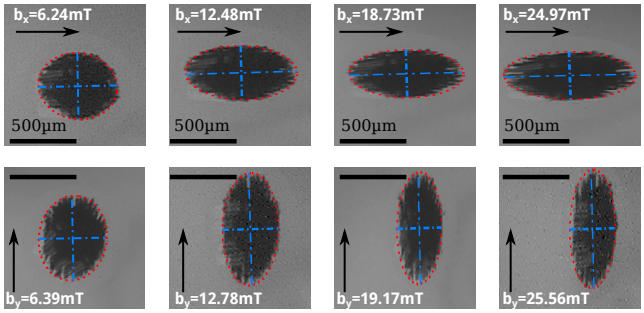

Fig. 7. Example of bolus deformation under a magnetic field, along the x-axis (first row) and the y-axis (last row) in an aqueous solution of 50% of glycerin (solution-#3).

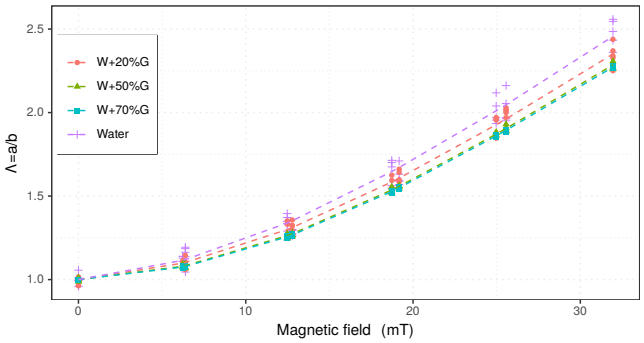

Fig. 8. The aspect ratio $\Lambda = a/b$ of the bolus as function of the magnetic field in different liquid viscosity. Dashed line reports the mean values for the different viscosity.

interfacial tension behaviors reported by Afkhami et al. [18] for a ferrofluid in a solution of 100% glycerin is depicted. Our obtained results appear to be in a good agreement with the others studies [17, 18].

Fig. 10 illustrates the aspect ratio Λ as function of the magnetic Bond number $\mathcal{B}_{\mathrm{o}\mathbf{m}}$ computed from Eqs. (1) and (7). This result shows that the magnetic bolus deforms continuously along with the increasing of magnetic field $\mathbf{b}$. Especially, when surface energy dominates ($\mathcal{B}_{\mathrm{o}\mathbf{m}} < 1$) the aspect ratio tends to $\Lambda \to 1$. Secondly, as one can see, the viscosity $\rho_{f/m}$ of the surrounding medium does not significantly contribute to the relationship between the aspect ratio Λ and magnetic Bond number $\mathcal{B}_{\mathrm{o}\mathbf{m}}$.

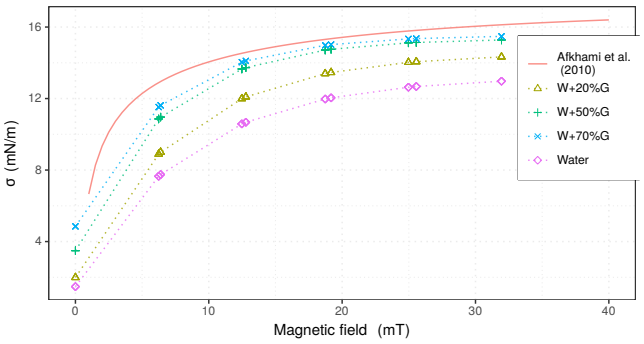

Fig. 9. The interfacial tension σ of the bolus as function of the magnetic field in various aqueous solution of glycerin. The solid line represents results from Afkhami et al. [18].

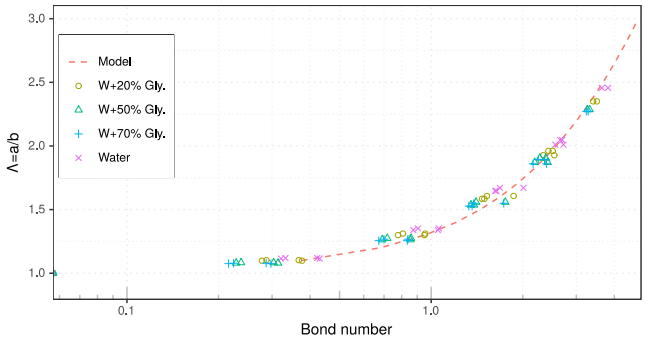

Fig. 10. Bolus aspect ration Λ as function of the magnetic Bond number for different aqueous solution viscosity. The red line (model) shows the curve computed from Eq. (7).

Contrarily, $\rho_{f/m}$ is involved in the relationship between the interfacial tension σ and $\mathcal{B}_{\mathrm{o}\mathbf{m}}$. Especially, the magnetic Bond number describes suitably either the aspect ratio thanks to Eq. (7), or the interfacial tension σ using (1). Finally, these preliminary results show that the proposed modeling suitably describes the behavior of the magnetic bolus in a low magnetic field.

C. Magnetic Bolus within a Rotating Magnetic Field

When applying a steady magnetic field $\mathbf{b}$ along a given direction θ, the shape of soft-microrobots deforms and its magnetization $\mathbf{m}$ tends to be aligned with $\mathbf{b}$, as depicted in Fig. 11. If the angle θ is changing, the magnetic moment of the bolus rotates to follow $\mathbf{b}$. For soft magnetic material, as with SPIO particles, and in a low magnetic field, the magnetic moment $\mathbf{m}$ slowly converges to $\mathbf{b}$. Hence, the soft-microrobot experiences the magnetic torque (3), that is equilibrated by the viscous torque (12) due to the friction of the droplet against the surrounding medium. The magnetization $\mathbf{m}$ has then a direction φ wrt. the easy axis of the soft-microrobot (see Fig. 2(c)). Specifically, the angle φ increases, and $\mathbf{m}$ is no longer aligned with neither the main direction of the soft-microrobot nor with $\mathbf{b}$, as shown in the inlet in Fig. 11 at time $t_1 = 100\,\mathrm{ms}$. This direction φ can be computed from the projection of the magnetic moment (4) and of the magnetic field $\mathbf{b}$, and we get:

$$\varphi = \tan^{-1}\left(\frac{1+\chi n_a}{1+\chi n_b}\tan\theta\right) \tag{15}$$

Moreover, in this work, mainly the two-dimensional (2D) behavior of the magnetic microrobot is considered, that is $b_z = 0$. Therefore, only a torque t_{mz} along the z-axis occurs, and Eq. (9) could be simplified as follows:

$$t_{mz} = \frac{V_{\mathrm{m}}\chi^2}{4\mu_0}\frac{|1-3n_a|}{(1+n_a\chi)(1+n_b\chi)}|\mathbf{b}|^2\sin(2\theta) \tag{16}$$

The magnetic torque is quadratic in $|\mathbf{b}|$, and is maximized when the phase lag is $\theta = 45°$, as mentioned by [25]. When the magnetic torque is equilibrated with the drag torque (12), the phase lag could be characterized from:

$$\sin(2\theta) = 24\eta_{f/m}\frac{\kappa_{\mathrm{rot}}}{\tau_m}\frac{\mu_0}{\chi^2}\frac{(1+n_a\chi)(1+n_b\chi)}{|1-3n_a|\ |\mathbf{b}|^2}\cdot\omega \tag{17}$$

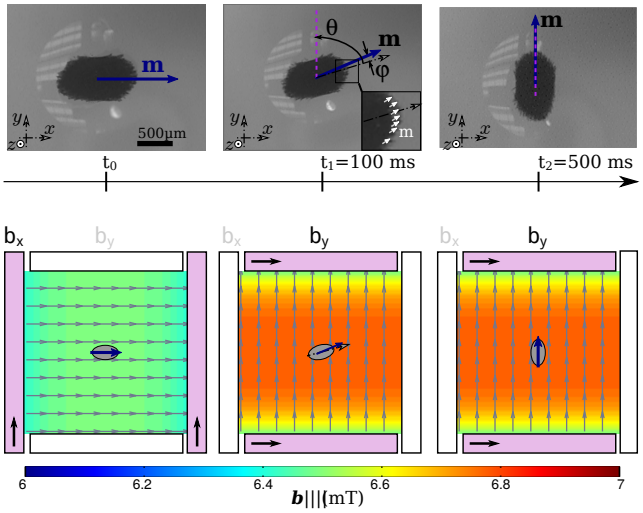

Fig. 11. A 90° rotation of the magnetic bolus in an aqueous solution with 50% of glycerin (solution-#3): (top row) snapshots of the bolus and (bottom row) rendering of the magnetic field **b** within the workspace.

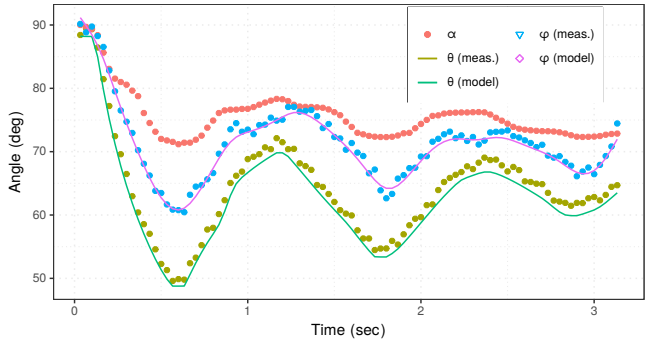

(a)

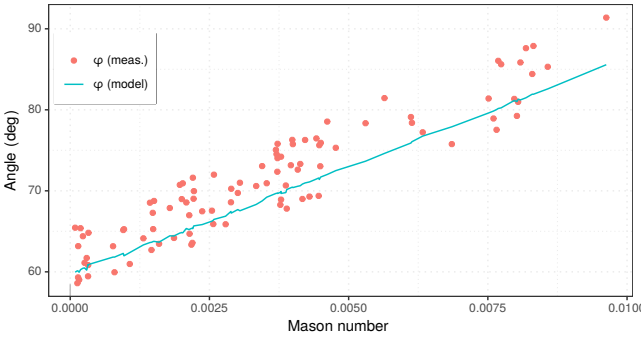

(b)

Fig. 12. Bolus-#B angle evolution in solution-#3 (50% water+ 50% glycerin): (a) comparison of measured values and models; and (b) the magnetization angle φ as function of the Mason number.

To characterize the magnetization direction φ and to assess the validity of the model, experiments within a rotating field was made. The Fig. 12(a) shows an example of the data for different angles in the case of the bolus-#B in the solution-#3. First, from the applied magnetic field, its measured direction θ is obtained. By analizing the data the 'measured' direction φ is determined (as the inlet in Fig. 11 at time $t_1 = 100\,\text{ms}$). Meanwhile, the models given by equations (15) and (17) can be evaluated. The data from measured values and models (15) and (17) are in good agreement. These results validate the presented modeling of deformable soft-magnetic microrobot.

Secondly, the magnetic and hydrodynamic forces are the dominant contributions that act on the magnetic bolus. These two interactions are typically grouped in the so called Mason number $\mathcal{M}_\text{n}$. This dimensionless parameter corresponds to the ratio of viscous to magnetic contributions. The literature defined different proportionality factors for $\mathcal{M}_\text{n}$ [26]. For the rotational behavior, the following definition is here considered:

$$\mathcal{M}_\text{n} = \frac{32\mu_0\eta_f\omega}{\chi^2|\mathbf{b}|^2} \tag{18}$$

The Fig. 12(b) depicts the evolution of the magnetization angle φ as function of the Mason forces. It should be noticed that Mason forces are strongly dominant. Hence, the ellipsoidal bolus orientation follows the magnetic field quickly and φ remains small. In contrast, for higher $\mathcal{M}_\text{n}$ values, the viscous friction slows down the motion of the bolus, whereas the SPIO particles tend to be aligned with the field **b**, leading to the increase of the magnetization angle φ. Compared to previous works attempting to model large deformable droplets (e.g. $L > 1$ mm) [17, 18, 19, 20], the proposed model allows to predict accurately the deformation of TMMCs at the microscale (e.g. $L < 0.5$ mm).

V. CONCLUSION

In this study, we have investigated the modeling and characterization of deformable soft-magnetic microrobot under various conditions. We have deeply characterized the magnetic behaviors of future TMMCs, with a particular attention to their deformation in response to an external magnetic field. It has been demonstrated experimentally that the shape and size of magnetic boluses strongly depends on the magnitude and direction of the applied magnetic field. The experimental results show that the observations follow quite well what was theoretically predicted by the models. This allows both to plan the shape of the magnetic bolus with respect to environmental conditions, and then to control its shape accordingly through the magnitude and direction control parameters. In future works, we will address these issues.

References

[1] C. Sun, J. S. H. Lee, and M. Zhang, "Magnetic nanoparticles in MR imaging and drug delivery," Adv. Drug Deliver. Rev., vol. 60, no. 11, pp. 1252–1265, Aug. 17, 2008.

[2] B. Wang, K. F. Chan, J. Yu, Q. Wang, L. Yang, P. W. Y. Chiu, and L. Zhang, "Reconfigurable Swarms of Ferromagnetic Colloids for Enhanced Local Hyperthermia," Adv. Funct. Mater., vol. 28, no. 25, p. 1 705 701, 2018.

[3] N. J. Darton, A. Ionescu, and J. Llandro, Eds., Magnetic Nanoparticles in Biosensing and Medicine. Cambridge University Press, 2019.

[4] V. F. Cardoso, A. Francesko, C. Ribeiro, M. Bañobre-López, P. Martins, and S. Lanceros-Mendez, "Advances in Magnetic Nanoparticles for Biomedical Applications," Adv. Healthc. Mater., vol. 7, no. 5, p. 1 700 845, 2018.

[5] A. Farzin, S. A. Etesami, J. Quint, A. Memic, and A. Tamayol, "Magnetic nanoparticles in cancer therapy and diagnosis," Adv. Healthc. Mater., vol. 9, no. 9, p. 1 901 058, 2020.

[6] H. Xie, M. Sun, X. Fan, Z. Lin, W. Chen, L. Wang, L. Dong, and Q. He, "Reconfigurable magnetic microrobot swarm: Multimode transformation, locomotion, and manipulation," Science Robotics, vol. 4, eaav8006, 28 2019.

[7] L. Mellal, D. Folio, K. Belharet, and A. Ferreira, "Modeling of Optimal Targeted Therapies Using Drug-Loaded Magnetic Nanoparticles for Liver Cancer," IEEE Trans. Nanobiosci., vol. 15, no. 3, Apr. 2016.

[8] Z. Wu, L. Li, Y. Yang, P. Hu, Y. Li, S.-Y. Yang, L. V. Wang, and W. Gao, "A microrobotic system guided by photoacoustic computed tomography for targeted navigation in intestines in vivo," Science Robotics, vol. 4, eaax0613, 28 2019.

[9] D. Ahmed, D. Hauri1, A. Sukhov, D. Rodrigue, M. Gian, J. Harting, and B. Nelson, "Bio-inspired acousto-magnetic microswarm robots with upstream motility," Nature Machine Intelligence, vol. 3, pp. 116–124, 2021.

[10] L. Mellal, K. Belharet, D. Folio, and A. Ferreira, "Optimal structure of particles-based superparamagnetic microrobots: Application to MRI guided targeted drug therapy," J. Nanopart. Res., vol. 17, no. 2, pp. 1–18, 2015.

[11] H.-W. Huang, M. S. Sakar, A. J. Petruska, S. Pané, and B. J. Nelson, "Soft micromachines with programmable motility and morphology," Nature Communications, vol. 7, no. 1, p. 12 263, 1 Jul. 22, 2016.

[12] A. L. Lewis, M. V. Gonzalez, A. W. Lloyd, B. Hall, Y. Tang, S. L. Willis, S. W. Leppard, L. C. Wolfenden, R. R. Palmer, and P. W. Stratford, "DC Bead: In Vitro Characterization of a Drug-delivery Device for Transarterial Chemoembolization," Journal of Vascular and Interventional Radiology, vol. 17, pp. 335–342, 2, Part 1 Feb. 1, 2006.

[13] J. Palacci, S. Sacanna, A. P. Steinberg, D. J. Pine, and P. M. Chaikin, "Living Crystals of Light-Activated Colloidal Surfers," Science, vol. 339, no. 6122, pp. 936–940, Feb. 22, 2013.

[14] F. Ma, S. Wang, D. T. Wu, and N. Wu, "Electric-field–induced assembly and propulsion of chiral colloidal clusters," PNAS, vol. 112, no. 20, pp. 6307–6312, May 19, 2015.

[15] J. Yu, L. Yang, and L. Zhang, "Pattern generation and motion control of a vortex-like paramagnetic nanoparticle swarm," The Int. J. Robot. Res., vol. 37, no. 8, pp. 912–930, Jul. 1, 2018.

[16] L. Yang and L. Zhang, "Motion Control in Magnetic Microrobotics: From Individual and Multiple Robots to Swarms," Annual Review of Control, Robotics, and Autonomous Systems, vol. 4, no. 1, null, 2021.

[17] J.-C. Bacri, D. Salin, and R. Massart, "Study of the deformation of ferrofluid droplets in a magnetic field," J. Physique Lett., vol. 43, no. 6, pp. 179–184, 1982.

[18] S. Afkhami, A. Tyler, Y. Renardy, M. Renardy, T. St Pierre, R. Woodward, and J. Riffle, "Deformation of a hydrophobic ferrofluid droplet suspended in a viscous medium under uniform magnetic fields," J. Fluid Mechanics, vol. 663, pp. 358–384, 2010.

[19] R. Probst, J. Lin, A. Komaee, A. Nacev, Z. Cummins, and B. Shapiro, "Planar steering of a single ferrofluid drop by optimal minimum power dynamic feedback control of four electromagnets at a distance," Journal of Magnetism and Magnetic Materials, vol. 323, no. 7, pp. 885–896, Apr. 2011.

[20] X. Fan, X. Dong, A. C. Karacakol, H. Xie, and M. Sitti, "Reconfigurable multifunctional ferrofluid droplet robots," PNAS, vol. 117, no. 45, pp. 27 916–27 926, Nov. 10, 2020.

[21] L. D. Landau, J. Bell, M. Kearsley, L. Pitaevskii, E. Lifshitz, and J. Sykes, Electrodynamics of continuous media. 1984, vol. 8.

[22] J. A. Osborn, "Demagnetizing Factors of the General Ellipsoid," Phys. Rev., vol. 67, no. 11-12, pp. 351–357, Jun. 1, 1945.

[23] E. M. Purcell, "Life at low Reynolds number," American Journal of Physics, vol. 45, no. 1, pp. 3–11, 1977.

[24] J. R. Melcher, Continuum electromechanics. MIT press Cambridge, 1981, vol. 2.

[25] J. J. Abbott, O. Ergeneman, M. P. Kummer, A. M. Hirt, and B. J. Nelson, "Modeling magnetic torque and force for controlled manipulation of soft-magnetic bodies," IEEE Transactions on Robotics, vol. 23, no. 6, pp. 1247–1252, 2007.

[26] S. Melle, O. G. Calderón, M. A. Rubio, and G. G. Fuller, "Microstructure evolution in magnetorheological suspensions governed by mason number," Physical Review E, vol. 68, no. 4, p. 041 503, 2003.